First Experiments and Commissioning of the ORCHID Nozzle Test Section

Beltrame, Fabio; Head, Adam J.; De Servi, Carlo; Pini, Matteo; Schrijer, Ferdinand; Colonna, Piero

DOI
10.1007/978-3-030-69306-0_18

Publication date
2021

Document Version
Final published version

Published in
NICFD 2020: Proceedings of the 3rd International Seminar on Non-Ideal Compressible Fluid Dynamics for Propulsion

Citation (APA)
Beltrame, F., Head, A. J., De Servi, C., Pini, M., Schrijer, F., & Colonna, P. (2021). First Experiments and Commissioning of the ORCHID Nozzle Test Section. In M. Pini (Ed.), *NICFD 2020: Proceedings of the 3rd International Seminar on Non-Ideal Compressible Fluid Dynamics for Propulsion* (pp. 169-178). (ERCOFTAC Series; Vol. 28). Springer. https://doi.org/10.1007/978-3-030-69306-0_18

First Experiments and Commissioning of the ORCHID Nozzle Test Section

Fabio Beltrame[1], Adam J. Head[1(✉)], Carlo De Servi[2], Matteo Pini[1], Ferdinand Schrijer[1], and Piero Colonna[1]

[1] TU Delft, Delft, Netherlands
{f.beltrame,a.j.head,m.pini,f.f.j.Schrijer,p.colonna}@tudelft.nl
[2] VITO, Mol, Belgium
carlo.deservi@vito.be

Abstract. This paper reports one of the initial NICFD experiments in the nozzle test section of the ORCHID aimed at providing accurate data for the validation of flow solvers, albeit, at this stage of the research, the focus is limited to inviscid phenomena. Notably, a series of schlieren photographs displaying Mach waves in the supersonic flow of the dense vapor of siloxane MM were obtained and are documented here for the commissioning experiment, namely, for inlet conditions corresponding to a stagnation temperature and pressure of $T_0 = 252\ ^\circ\mathrm{C}$ and $P_0 = 18.4$ bara. At these inlet conditions the compressibility factor of the fluid is $Z_0 = 0.58$. The digital processing of the schlieren images allowed to estimate multiple angles formed by the Mach waves stemming from the upper and lower nozzle surfaces because of the infinitesimal density perturbations generated by the, albeit small, roughness of the metal surfaces. These values are related to the local Mach number by a simple geometric relation. Moreover, the total expanded uncertainty in the Mach number was computed. This information together with the estimate of the average Mach number was used for a first assessment of the capability of evaluating NICFD effects occurring in a dense organic vapor flow of MM by comparison with the results of CFD simulations. The outcome of the comparison was satisfactory. It can thus be inferred that the nozzle test section has been commissioned and it is ready for experimental campaigns in which its full potential in terms of measurements accuracy, repeatability, and operational flexibility will be exploited.

Keywords: Schlieren measurements · Data processing · Error identification · Uncertainty estimation

1 Introduction

The computer simulation of compressible flows is critical for a large variety of scientific studies and engineering purposes. CFD codes have reached a remarkable level of accuracy. A vast amount of accurate experimental data is available for their verification and validation [10], as well as, in principle, to improve their accuracy via, e.g., calibration. However, all this body of experimental work deals to an almost complete extent with aerodynamics or classical and ideal gas dynamics. There is limited data available

M. Pini et al. (Eds.): NICFD 2020, ERCOFTAC Series 28, pp. 169–178, 2021.
https://doi.org/10.1007/978-3-030-69306-0_18

for geometries and flows typically encountered in ORC expanders and, more in general, for those constituting the research subject of Non-Ideal Compressible Fluid Dynamics (NICFD), such as transcritical expansions close to the critical point and compressible two-phase flows. Although first experimental results on non-ideal compressible effects in supersonic flows of dense organic vapours have been recently published, see Ref. [11, 12, 14], the data in the literature remain insufficient in terms of quantity and quality for the validation of modern CFD software. For this reason, the Organic Rankine Cycle Hybrid Integrated Device (ORCHID) has been conceived and realized to provide both accurate experimental data for paradigmatic NICFD benchmark flows and, in a second phase of the research, measurements for turbomachinery operating partly or entirely in the NICFD regime. The ORCHID is a continuous operating-type vapor tunnel capable of realizing a high-temperature organic Rankine cycle (ORC) with different working fluids in numerous operating conditions [7]. One of the test sections, namely, the nozzle test section, has been realized to 1) generate paradigmatic supersonic flows, similarly to what is done for classical and ideal gas dynamics, but for flows in the NICFD regime, namely a simple flow in a convergent divergent either empty or with an obstacle inserted to generate shock waves, and 2) to accurately measure quantities for validation of CFD codes capable of simulating NICFD flows. This paper describes the initial experiments carried out during the commissioning of the ORCHID nozzle test section. In particular, datasets have been generated for: i) the total conditions at the inlet and outlet of a planar nozzle, and, ii), thanks to schlieren imaging, Mach lines over almost the entire length of the diverging part of the nozzle. These quantities are sensitive to NICFD effects because of the influence of both volumetric and caloric thermodynamic properties of the fluid. Furthermore, all error sources influencing the measurement of the Mach number have been identified and subsequently quantified, including the uncertainties arising from the post processing method of the schlieren images.

The paper is structured as follows. Section 2 presents a description of the primary components of the nozzle TS. Furthermore, the schlieren layout and measurement procedure together with the specifications of the commissioning experiment are defined. In Sect. 3 the schlieren post processing method and the uncertainty estimation of the experiment error sources is presented. Section 4 reports the average midline Mach number distribution in the nozzle kernel region together with the associated uncertainties. The results are also compared with CFD predictions. The conclusions and an outlook for future work are presented in Sect. 5.

2 Nozzle Test Section: Layout and Schlieren Measurement Procedure

Figure 1a shows an isometric view of the ORCHID nozzle test section (TS), which consists of three primary compartments: the settling chamber (SC) which contains the flow conditioning devices such as honeycombs and screens; the nozzle housing (NH), which hosts a planar converging-diverging nozzle; and, the receiver (RC). The nozzle is made from two equal and removable profiles, which are inserted at the top and bottom of the nozzle housing. Figure 1b shows the diverging portion of this profile which has been designed with the method of characteristics [5]. The side walls of the nozzle

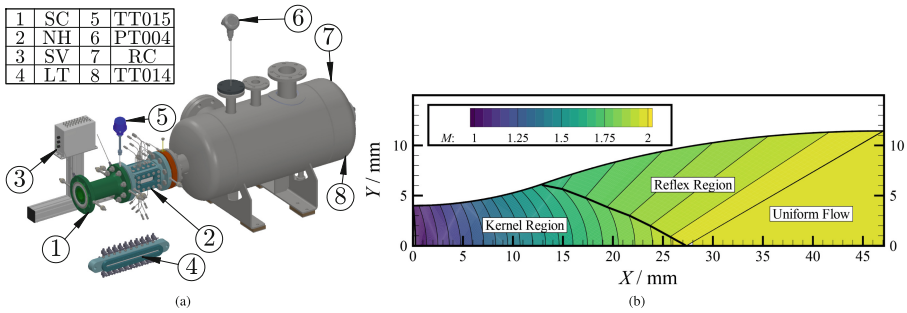

Fig. 1. (a). The primary components of the nozzle TS. SC: settling chamber; NH: nozzle housing; SV: Scanivalve; LT: liquid traps; RC: Receiver. **(b).** Flow Mach number in the diverging portion of the nozzle as calculated with the method of characteristics [5] for the MM working fluid at the design conditions: $T_0 = 252$ °C, $P_0 = 18.4$ bar and a back pressure of 2.1 bar. Taken from [6]. Fluid properties estimated with FLUIDPROP [4] Model = REFPROP [8].

are made from transparent windows which provide optical access. The test section is equipped with a Scanivalve (SV) DSA3218 pressure scanner which is used, in combination with pressure taps, to characterise the total pressure in the settling chamber and to measure the static pressures along the nozzle profile. To avoid the accumulation of condensate in the lines connecting the pressure taps to the Scanivalve, the pressure scanner is equipped with a purging system. Moreover, a specially engineered liquid trap (LT) allows to visualise vapor condensation during pressure measurements. As far as the total temperature is concerned, this is measured at the nozzle inlet (TT015) with a *Wika* PT100 transmitter. The expanded uncertainty is of Class A, i.e., $\pm 0.15 + 0.002\,|T|$ °C as per the EN 60751 standard. The same type of transmitter is also used to measure the temperature (TT014) in the receiver. Finally, the back pressure (PT004) is measured by a *Wika* UPT 20 pressure transmitter with an expanded uncertainty of ± 0.1 bar.

The adopted schlieren layout is a two-lens flat mirror z-type configuration. The schlieren equipment, then, consists of a light source (cold white LED from Thorlabs), a pinhole (diameter 0.2 mm), two collimating and schlieren lenses (diameter 116 mm, focal length 1524.7 mm), two mirrors $(L \times H = 127 \times 178)$ mm, a knife edge and a camera. This equipment is mounted on three separate rigid structures which ensure the correct alignment of all components, see Ref. [6]. The camera used to image the flow field is a BOBCAT IGV-B1610 16bit CCD camera with a maximum resolution of 1628×1236 pixels.

The operating conditions chosen for the commissioning experiments corresponds to those considered as design point of the ORCHID Balance of Plant (BoP) and nozzle test section. The targeted conditions are reported in Table 1 while Fig. 2 displays the thermodynamic states identifying the expansion process in the nozzle under the hypothesis of an isentropic adapted flow. When the ORCHID BoP warm-up is completed and the operating conditions have stabilized around the values of total inlet pressure and temperature chosen for the experiment, the nozzle test section is opened. Around twenty

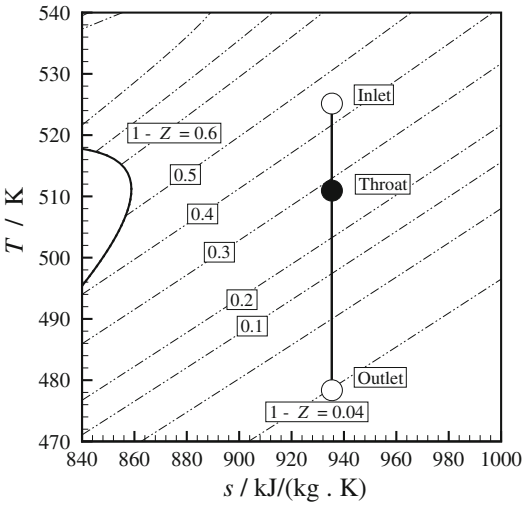

Fig. 2. $T - s$ diagram showing the isentropic expansion of the commissioning experiment with contours of 1-Z.

Table 1. The target boundary conditions of the commissioning experiment PR.025-NT.002.

Fluid	Tot. temp. TT015/°C	Tot. press. $P_{SV}001$/bara	Comp. F. Z_t
MM	252	18.4	0.56
Back p. PT004/bara	Outlet Mach. M_2	Mass flow FT001/kg/s	
2.1	2	1.145	

minutes are then required to stabilize again the nozzle inlet conditions, provided that the test section was preheated before to sufficiently high temperature (say 180 °C for NICFD experiments with MM). During this settling period, the back pressure PT004 of the nozzle is set to the desired value. Afterwards, the schlieren image acquisition is activated. An image acquisition frequency 25 Hz is appropriate and allows to achieve statistical convergence of the measure quantities, provided that the flow field and boundary conditions are sufficiently steady. Approximately 2,000 images are recorded in order to characterise the Mach number along the midplane of the nozzle. Then the inlet and outlet valves of the nozzle test section are closed and an image of the empty nozzle is taken for the postprocessing of the schlieren images.

3 Schlieren Images Postprocessing and Measurement Uncertainty

The method for the Mach number extraction and uncertainty evaluation from a schlieren image dataset consists of the following main steps: first, the entire image dataset is enhanced by aligning each single frame to the first schlieren image to compensate for possible shifts and rotations in the reference frame of each picture caused by vibrations in the test section. This operation is performed in the DaVis software 8.3.0 from Lavision. Second, a Mach line extraction algorithm implemented in Matlab is applied to evaluate the slope of the Mach waves with respect to the local flow velocity (Mach line angle μ) at different axial positions along the nozzle midplane for a sequence of schlieren images. The code evaluates also the total expanded uncertainty associated with the estimated Mach line angles. The accuracy of the extracted information is, then, assessed by verifying flow symmetry and steadiness. The flow is deemed symmetric if the difference in the angles of the Mach lines converging to the same location along

the nozzle midplane is smaller than a given threshold, i.e. the smaller total expanded uncertainty estimated by the tool for the angles of the two intersecting Mach lines. As far as the steadiness of the flow is concerned, this check is performed by verifying that the mean and standard deviations of the Mach line angles extracted by the algorithm remain constant as the number of processed images increases. For the process run under consideration, the number of images required to obtain a constant mean and standard deviation is approximately one thousand. Given the acquisition frequency of the camera, i.e. 25 Hz, this corresponds to the analysis of 40 s of flow history. Finally, if the flow symmetry and steadiness is verified, the estimated Mach line angles in the diverging part of the nozzle are used to calculate, for each image, the corresponding Mach number distribution according to the Mach equation

$$M = \frac{1}{\sin(\mu)}. \tag{1}$$

Describing more in detail the Mach line extraction algorithm, the first operation consists in applying a 2D Gaussian filter to the processed image in order to remove noise, like darker and lighter spots, which might be due, for example, to spurious reflections. Subsequently, the Canny edge detection algorithm is used to identify the contours of the Mach lines, by computing the intensity gradients of the image with respect to a given threshold. The outcome of the Canny algorithm is a binary image which is then divided into sub-images called interrogation windows centered on the nozzle midplane. The Mach lines tend to bend at increasing distance from the midplane due to 2D flow effects, whose intensity augments the closer the location to the nozzle throat. The interrogation window dimension is, then, adapted to ensure that the maximum line curvature is lower than the angular resolution, which implies that no curvature effect are detectable in the portion of the image processed by the algorithm. This is achieved by specifying a window height to nozzle height ratio equal to 0.15. In the experiment at hand, the size of the interrogation windows (rows $\times$ columns), then, ranges from 45×50 pixels in the throat region to 60×70 pixels at the nozzle exit. Finally, the Hough transform [9] is applied to identify the lines which best fit the contours or edges detected by means of the Canny algorithm. More in detail, the Hough transform determines for each pixel of the selected interrogation window if a straight line with a specific orientation and distance from the origin r may pass through that pixel. The result of this process is a two-dimensional matrix called accumulator which ranks the different lines based on the number of pixels they fit. The number of columns and rows of the matrix is a function of the resolution set by the user to discretize, respectively, the inclination θ and the distance from the origin r of the lines. The greater the resolution, the larger the matrix. The cell in the matrix with the highest value represents the combination of θ and r which best fits the edges determined by the Canny algorithm and that identifies a candidate Mach line. In order to ensure the detection of a Mach line and not a random number of collinear points, only the line with the highest value in the accumulator and with a length above a specified threshold is selected. For more details about the implementation of the Mach line angle detection algorithm, the interested reader is referred to Ref [2].

Figure 3a shows the average Mach lines superimposed on the first schlieren image. The domain of interest is the so-called kernel region of the supersonic flow, where the non-ideal gas dynamic effects are more prominent. Notice that the refractive index

changes significantly due to the large variation in fluid density between the throat and the end of the kernel region, which translates to a substantial change in contrast. It occurs that the image tones become darker and darker moving from the nozzle outlet towards the inlet, up to the point that the light deviation exceeds the schlieren system measuring range in the area close to the throat. For this reason, it was not possible to estimate the flow Mach number in that region of the images. The contrast is insufficient to allow a consistent identification of the Mach lines over the dataset: the computed standard deviation of line angles in interrogation windows close to the throat exceeds a predefined threshold, namely three times the total expanded uncertainty calculated for the Mach line angles in the window that follows the one of interest with respect to the flow direction.

Primary error sources in the measurement of the flow Mach number include i) a misalignment of the optical system, ii) the finite and discrete resolution of the CCD sensor of the camera, and iii) approximations introduced by the implemented post-processing algorithms. In this regard, the total expanded uncertainty in the flow Mach number can be expressed as

$$U_M = \sqrt{(U_{\mathrm{M,data}})^2 + (U_{\mathrm{M,ext}})^2 + 2\rho_{\mathrm{data,ext}} \cdot U_{\mathrm{M,data}} \cdot U_{\mathrm{M,ext}}}\,, \tag{2}$$

where $U_{\mathrm{M,data}}$ is the uncertainty due to random effects, while $U_{\mathrm{M,ext}}$ is the uncertainty related to the algorithm used for processing the schlieren images and $\rho_{\mathrm{data,ext}}$ is the Pearson correlation coefficient between the two error sources. $U_{\mathrm{M,data}}$ can be estimated based on the standard deviation of the flow Mach angle resulting from the statistical processing of the whole image dataset and assuming a 95% confidence interval. $U_{\mathrm{M,ext}}$ can be evaluated as a function of the corresponding uncertainty in the measurement of the Mach line angle. In particular, $U_{\mathrm{M,ext}}$ may be calculated by propagating the uncertainty $U_{\mu,\mathrm{ext}}$ through the Mach equation, i.e.

$$U_{M,\mathrm{ext}} = M\sqrt{M^2 - 1}U_{\mu,\mathrm{ext}}, \tag{3}$$

where the multiplicative factor for $U_{\mu,\mathrm{ext}}$ is derived by evaluating the derivative of the Mach number with respect to the Mach line angle $|\frac{dM(\mu)}{d\,\mu}|$ [2]. Equation 3 implies that the uncertainty on the flow Mach number increases from the throat to the exit of the nozzle. The uncertainty associated with the estimation of the Mach angle $U_{\mu,ext}$ is, in turn, estimated as

$$U_{\mu,ext} = \sqrt{AR_{95}^2 + U_{\mathrm{Hough,res}}^2}, \tag{4}$$

where $U_{\mathrm{Hough,res}}$ is the Hough transform (see [9]) angular discretization uncertainty, which is assumed to be half of the discretization step for the line orientation $\Delta\theta$ considered in the accumulator. On the other hand, AR_{95} is the 95% confidence level uncertainty on the detected angle due to the image resolution, or, in other words, the angular resolution associated with a given interrogation window. The finite number of pixels of the image inherently introduces an approximation on the line angle, which tends to increase the shorter the Mach lines [2]. As the size of the interrogation windows is not constant, the length of the detected Mach lines varies, thus the minimum angle that can

be identified. The angular resolution is, indeed, equal to the arctangent of the inverse of the detected line length. AR_{95} is, then, determined for each interrogation window by calculating the average angular resolution and adding to this term two times the line length standard deviation propagated through the angular resolution equation.

Also the position at which the flow Mach number is measured is affected by uncertainty. First, distances in the image are in pixels and need to be converted into linear distances. The uncertainty associated to this operation depends on the adopted pixel-to-meter conversion ratio, here evaluated by dividing the throat height, measured with the caliper before the experiment, by the length in pixels of the channel height estimated in correspondence of the throat. Second, a Mach line identified by the Hough transform is *a priori* assumed passing through the center of the interrogation window processed by the algorithm. The corresponding uncertainty, assuming a 100% containment level and a uniform distribution, is equal to half of the interrogation window width.

4 Experiment Versus Numerical Simulation

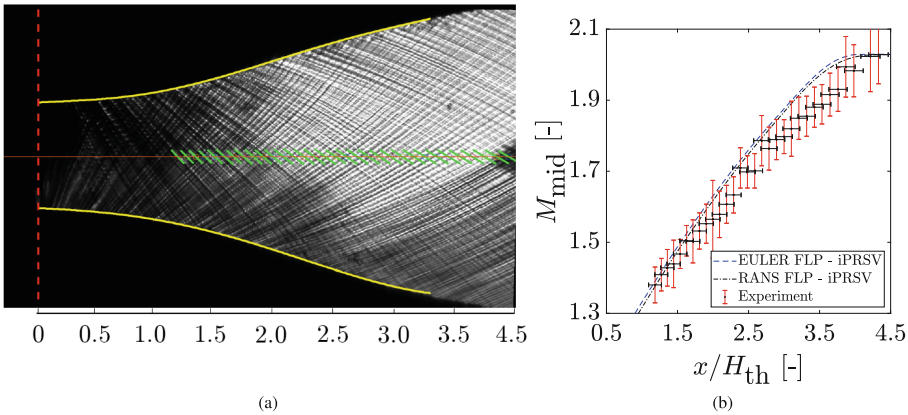

Fig. 3. (a). Average extracted Mach lines superimposed on the first schlieren image. **(b).** Comparison between the measured flow Mach number with the corresponding total expanded uncertainty and two different numerical predictions. Taken from [6].

Figure 3b shows the comparison between two numerical predictions against the Mach number distribution along the nozzle mid-plane obtained experimentally. The experimental data is complemented with the estimated total expanded uncertainty. The axial coordinate x in the figure, which represents the distance along the nozzle mid-plane from the throat, is normalized with respect to the nozzle throat height H_{th}. The total expanded uncertainty on the extracted Mach number ranges from $M = 1.38 \pm 0.05$ to 2.03 ± 0.082 at positions $x/H_{\mathrm{t}} = 1.18$ and 4.33, respectively. The numerical solutions of the flow-field in the ORCHID nozzle are obtained using the open-source flow solver

SU2 for a 2D half-nozzle with symmetry conditions along the midplane. The generalized Roe scheme with second-order MUSCL reconstruction is used for the computation of the advective fluxes. The total inlet conditions assumed in the CFD model correspond to the average total pressure and temperature measured at the nozzle inlet during the experimental run once steady flow conditions established. Their values are $P_{0,\text{avg}} = 18.36 \pm 0.18$ bar, $T_{0,\text{avg}} = 252.4 \pm 0.69$ °C. The pressure measured at the nozzle outlet is $P_{\text{b,avg}} = 2.06 \pm 0.25$ bar. The thermo-physical properties of the siloxane MM have been computed by an external fluid properties library [4]. In particular, the thermodynamic properties of the fluid are estimated by using the iPRSV cubic equation of state. The transport properties are calculated with the Chung's transport model. Furthermore, a fourth order polynomial function of the temperature is used for the ideal gas isobaric heat capacity [13]. For the inviscid simulations, the Euler implicit time marching scheme with a CFL of 20.0 is used. A grid convergence study based on the methods given in Ref. [1,3] was performed to determine a proper size of the unstructured mesh. This indicates that a grid of 10,000 elements provides mesh independent results and, as such, the numerical uncertainty can be deemed negligible. Regarding the RANS simulation, turbulence effects have been modeled by the Shear-Stress Transport (SST) closure. The calculations have been run with a high-order resolution scheme for the advective and turbulent fluxes. Moreover, additional mesh cells are used to resolve the boundary layer with $y^+ < 1$ along the nozzle walls. Finally, all the CFD simulations were performed with a workstation equipped with an Intel i7-8750H (2.21 GHz, 6 cores).

The predicted Mach numbers match reasonably well with the experimental results, in particular at the initial stages of the expansion. The difference between the average flow Mach number and the RANS prediction at position $x/H_{\text{th}} = 1.2$ is less than 0.6%. The maximum deviation is 4.4% of the experimental Mach number, and occurs at position $x/H_{\text{th}} = 3.54$. The simulation results are slightly above the upper bound of the experimental uncertainty. This deviation tends to increase as the Mach number augments, i.e. towards the nozzle exit. Figure 3b shows also that the RANS simulation predicts lower values for the flow Mach number along the expansion process when compared to the EULER simulations. The differences between the two numerical simulations are, however, very small. The reasons for the discrepancy between the prediction of the CFD models and the experimental data are most likely owed to the fact that, the former do not account for 3D effects, such as the boundary layer development on the flat glass window panes, which causes a reduction in the nozzle area ratio. Furthermore, thermal effects are not negligible. A different dilation of the nozzle housing with respect the nozzle profile may alter the nozzle throat height during the test runs, thus modifying the nozzle flow area. This effect will be assessed in future experiments.

As it can be noticed from Fig. 3b, the total uncertainty on the flow Mach number increases towards the exit of the nozzle. This occurs despite the random uncertainty $U_{\text{M,data}}$ is almost constant in the analyzed portion of the flow, with a slight increase towards the nozzle throat where lines are less visible and the quality of the images decreases. Also the uncertainty associated to the Mach line angles, U_μ, is almost constant, at least as long as the brightness level of the image is constant and the images are sharp. The reason of the trend in the total uncertainty in Fig. 3b is, then, the increase of

$U_{M,ext}$, in accordance with Eq. 3, which shows that uncertainties in the μ angle increase with the flow for Mach number for values of this quantity greater than 1.3.

5 Conclusions

This paper reported initial results of the ORCHID nozzle commissioning experiments. A sequence of schlieren images allowed to characterise the Mach lines associated with the expansion of MM in a thermodynamic region where the properties of the vapour substantially deviate from those of an ideal gas. An *ad-hoc* methodology has been implemented to process the schlieren images and to estimate the flow Mach number on the nozzle midplane and its total uncertainty. These data have been, then, used to make a preliminary assessment of the predictive capabilities of the SU2 flow solver for NICFD applications. In particular, predicted Mach numbers matched well with the experimental results at the initial stages of the expansion. Deviations towards the end of the kernel region may be due to viscous phenomena not accounted for in the CFD models and thermal dilation effects in the nozzle test section which may alter the throat area. It was also observed that the uncertainty on the flow Mach number evaluated experimentally strongly depends on the uncertainty associated with the post-processing of the schlieren images, where the main source of error is the limitation on the angular resolution of the Mach lines which, in turn, depends on the pixel resolution of the images and the size of the Hough transform search space.

Acknowledgments. The authors would like to express their gratitude to Liam Bills for producing the simulation results with SU2.

References

1. American Society of Mechanical Engineers (ASME): Standard for verification and validation in computational fluid dynamics and heat transfer. Technical report V&V20-2009, ASME (2009)
2. Beltrame, F.: Accuracy assessment of the SU2 flow solver for non-ideal organic vapor supersonic expansions using experimental data. Master's thesis, TU Delft, Politecnico di Torino (2020)
3. Celik, I.B., Ghia, U., Roache, P.J., Freitas, C.J., Coleman, H., Raad, P.E.: Procedure for estimation and reporting of uncertainty due to discretization in CFD applications. J. Fluids Eng. **130**(7), 7 (2008)
4. Colonna, P., van der Stelt, T.P., Guardone, A.: FluidProp (version 3.0): A program for the estimation of thermophysical properties of fluids (2012)
5. Guardone, A., Spinelli, A., Dossena, V.: Influence of molecular complexity on nozzle design for an organic vapor wind tunnel. J. Eng. Gas Turbine Power **135**(4), 042307 (2013)
6. Head, A.J.: Novel experiments for the investigation of non-ideal compressible fluid dynamics: the ORCHID and first results of optical measurements. Ph.D. thesis, Delft University of Technology (2021)
7. Head, A.J., De Servi, C., Casati, E., Pini, M., Colonna, P.: Preliminary design of the ORCHID: a facility for studying non-ideal compressible fluid dynamics and testing ORC expanders. In: ASME Turbo Expo, number GT2016-56103, p. 14 (2016)

8. Lemmon, E.W., Huber, M.L., McLinden, M.O.: NIST standard reference database 23: reference fluid thermodynamic and transport properties-REFPROP, version 9.1. Technical report, National Institute of Standards and Technology, Standard Reference Data Program, Gaithersburg (2013)
9. Lo, R., Tsai, W.: Gray-scale Hough transform for thick line detection in gray-scale images. Pattern Recogn. **28**(5), 647–661 (1995)
10. Roache, P.J.: Verification and Validation in Computational Science and Engineering. Hermosa Publishers, Albuquerque (1998)
11. Robertson, M., Newton, P., Chen, T., Costall, A., Martinez-Botas, R.: Experimental and numerical study of supersonic non-ideal flows for organic rankine cycle applications. J. Eng. Gas Turbines Power **142**(8) (2020). https://doi.org/10.1115/1.4046758
12. Spinelli, A., Cammi, G., Gallarini, S., Zocca, M., Cozzi, F., Gaetani, P., Dossena, V., Guardone, A.: Experimental evidence of non-ideal compressible effects in expanding flow of a high molecular complexity vapor. Exp. Fluids **59**(8), 126 (2018). ISSN 1432-1114
13. van der Stelt, T.P., Nannan, N.R., Colonna, P.: The iPRSV equation of state. Fluid Phase Equilibria **330**, 24–35 (2012)
14. Zocca, M., Guardone, A., Cammi, G., Cozzi, F., Spinelli, A.: Experimental observation of oblique shock waves in steady non-ideal flows. Exp. Fluids **60**(6), 101 (2019)